ACS Photonics

pubs.acs.org/journal/apchd5

Article

Dynamically Selective and Simultaneous Detection of Spin and Orbital Angular Momenta of Light with Thermoresponsive Self-Assembled Chiral Superstructures

Yi-Heng Zhang, Peng Chen,* Chun-Ting Xu, Lin Zhu, Xin-Yue Wang, Shi-Jun Ge, Wei Hu, and Yan-Qing Lu*

Cite This: *ACS Photonics* 2022, 9, 1050−1057

Read Online

ACCESS | Metrics & More | Article Recommendations | Supporting Information

ABSTRACT: Featuring a self-assembled helical nanostructure and external stimuli-responsive chiral photonic band gap, cholesteric liquid crystals (CLCs) create more opportunities in harnessing multiple degrees of freedom of light, especially the spin and orbital angular momenta (SAM/OAM). Here, we propose and demonstrate an innovative method for a dynamically selective and simultaneous detection of SAM and OAM of light *via* two cascaded CLC superstructures with thermal controllability and opposite chirality. By independently regulating their temperatures, on-demand selective detection for the intended wavelength and spin eigenstate is achieved with high efficiency and broadband tunability. The information of the desired angular momenta is vividly identified by the reflected diffraction patterns from cascaded chiral superstructures, while the nondetected components are preserved in the transmitted light. This indicates an *in situ* and nondestructive manner and may facilitate advanced optical manipulation, imaging, and information (de)multiplexing. This work brings important insights into the design, construction, and application of self-assembled chiral nanostructures, promoting multiple and active functionalities in diverse intelligent devices.

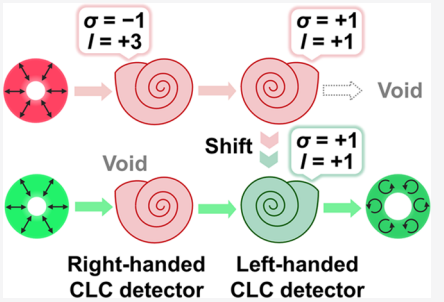

KEYWORDS: *self-assembled chiral superstructures, orbital angular momentum of light, geometric phases, vector vortex beams, thermal response*

Nature has evolved omnipresent chirality, for instance, in the double helix of DNA carrying genetic information and in the beetle exoskeletons exhibiting brilliant structural colors.[1,2] These inspire scientists from various communities to mimic the chirality in nature and develop chiral nanostructures with manifold geometries for addressing diverse challenges.[3−5] Among them, cholesteric liquid crystals (CLCs) are very special and intriguing building blocks. Anisotropic liquid crystal (LC) molecular units self-assemble into an elegant helical organization, which establishes a bridge between nanoscale molecules and mesoscopic structures on the wavelength scale.[6,7] Thanks to the involved periodicity of the refractive index in such a helical nanostructure, the CLC forms a one-dimensional self-organized chiral photonic structure, giving rise to a Bragg reflection (*i.e.*, photonic band gap) with strong selectivity of circular polarization.[8,9] Polarization is a basic degree of freedom of light. In particular, circular polarizations are the orthogonal eigenstates associated with the so-called spin angular momentum (SAM) of light.[10] Left/right circularly polarized (LCP/RCP) light carries an SAM of $\sigma\hbar$, where $\sigma = +1/-1$.

In addition to the SAM, light can also carry an orbital angular momentum (OAM)[11,12] of $l\hbar$, accompanied by a spiral phase profile with the topological charge l. The tensor product of SAM- and OAM-state spaces describes a set of nonseparable modes, typically as vector vortex beams (VVBs).[13] They have triggered various applications including optical manipulation,[14,15] laser manufacturing,[16] sensing,[17] and super-resolution imaging.[18] In the last decade, the multiplexing of multiple degrees of freedom of light, including wavelength, polarization, and theoretically infinite OAM states, has accelerated high-capacity optical communications[19,20] and high-dimensional quantum informatics,[21] where the efficient demultiplexing of independent information channels plays a crucial role. Nevertheless, dynamically controllable and simultaneous detection of the SAM and OAM of light is still facing formidable challenges when using a traditional single optical element.[22−25] Fortunately, owing to the natural spin selectivity induced by its helix chirality, the cascade of CLCs with opposite handedness is a promising candidate for the simultaneous processing of orthogonal SAM eigenstates. Very recently, the reflective geometric phase from CLCs has been

Received: December 30, 2021
Published: January 27, 2022

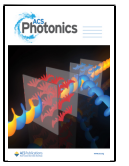

https://doi.org/10.1021/acsphotonics.1c02017
ACS Photonics 2022, 9, 1050−1057

revealed[26−28] and featured by broadband high efficiency, spin-selective modulation, and spin-determined propagation, which promotes powerful wave front engineering.[29−32] Moreover, the self-organization of CLCs is highly sensitive to diverse external stimuli, such as electric/magnetic fields,[33,34] heat,[35−37] light,[38−42] and relative humidity.[43] If delicately designed optical nanostructures were imprinted into CLC chiral superstructures and their stimuli-responsive self-assembly was fully extracted, controllably selective and simultaneous discrimination of spin and orbital angular momenta of light could be rationally expected.

In this work, we propose a method for the desired SAM and OAM detection based on two cascaded CLC superstructures with thermoresponsivity and opposite chirality. The SAM is detected by spin-selective Bragg reflection, and the OAM is identified by geometric phase modulation from a distorted-grating-encoded chiral superstructure. Both angular momenta are clearly distinguished by the absence/presence and the dark fringes of reflected diffraction patterns. By independently regulating the temperature of the two chiral superstructures, each photonic band is shifted to include or exclude the incident wavelength. Thus, we can achieve on-demand selective detection corresponding to the intended wavelength and SAM eigenstate. Notably, the nondetected component of incident light just transmits and maintains its original SAM and OAM characteristics, indicating an *in situ* and nondestructive way. Our work supplies an efficient implement for the controllable and simultaneous manipulation of the angular momenta of light and extends the applications of self-assembled chiral nanostructures.

RESULTS AND DISCUSSION

The proposed concept of dynamically selective and simultaneous detection of SAM and OAM is schematically illustrated in Figure 1a. It is composed of an RCP- and LCP-selective optical element with a carefully designed structure capable of OAM detection, symbolized by a dextral and sinistral shell, respectively. The operating wavelength of each element is tunable, denoted by the color of the shell. Accordingly, two detection schemes can be designed. "Joint detection" means the simultaneous identification of both SAMs and OAMs, under the condition that the wavelength of the incident light falls within the operating bands of both elements. Take the red VVB as an example, which is the superposition of an RCP and LCP optical vortex carrying SAMs and OAMs,[13,44] denoted as ($\sigma = -1, l = +3$) and ($\sigma = +1, l = +1$), respectively (Supporting Information, Text 1). The SAM of $\sigma = -1$ and the OAM of $l = +3$ are detected by the RCP-selective element, while $\sigma = +1$ and $l = +1$ are simultaneously detected by the LCP-selective element. On the contrary, if just one element operates at the incident wavelength, only the corresponding SAM and OAM information could be revealed, while the rest will be kept in the transmitted light without distortion. This scheme is named as "selective detection", which is vividly presented for the case of a green VVB in Figure 1a.

The RCP/LCP-selective element in the abovementioned design can be perfectly demonstrated with right/left-handed self-assembled chiral nanostructures. Compared with the traditional top-down micro−nanomachining technique,[45] intrinsic self-assembly and viscoelastic properties of CLC materials take advantage of the molecular interaction and arrangement, and thus, the hierarchical chiral superstructures can be constructed with a much higher efficiency and better

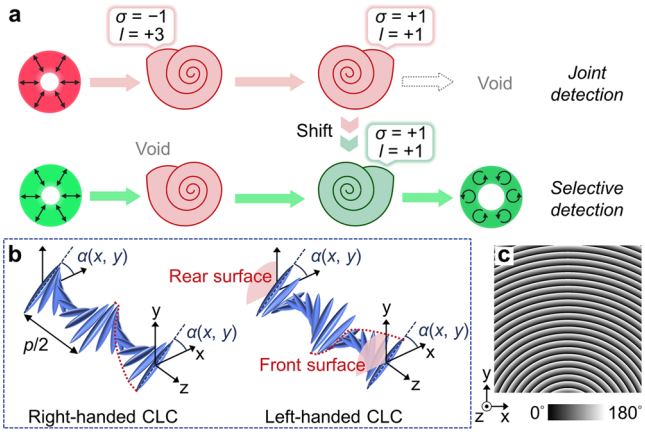

Figure 1. Conceptual illustration of the dynamically selective and simultaneous detection of the SAM and OAM of light. (a) Dextral/sinistral shell represents the RCP/LCP-selective optical element capable of OAM detection, whose color denotes the tunable operating wavelength. In the scheme of joint detection, both SAMs and OAMs are simultaneously detected. In the scheme of selective detection, one spin eigenstate is detected, while the orthogonal one is transmitted. The polarization distributions are depicted for incident and transmitted light. The detected SAM and OAM data are labeled. (b) Schematic of the right/left-handed CLC nanostructures. The blue rods denote LC molecules, and the red dashed line indicates the direction of the helix turn. z depicts the axis of the CLC helix, p is the helical pitch, and α is the orientation angle of the local LC director at the front/rear surface with respect to the x-axis. (c) Theoretically designed α distribution of a CLC distorted grating. The color variation from black to white indicates the orientation angle varying from 0 to 180°.

uniformity.[7,46] Figure 1b schematically shows CLC helixes with an orthogonal chirality and parallel molecule orientation at the front and rear surfaces. For the normal incident light propagating along the helical axis, the CLC chiral structure forms a Bragg photonic band within the wavelength range of $n_o p - n_e p$, where n_o/n_e is the ordinary/extraordinary refractive index, respectively, and p is the helical pitch.[8] The circularly polarized light with the same handedness as that of the chiral nanostructure is reflected, while the opposite one is totally transmitted. Notably, if the orientation angle of the local LC director at the front surface is α with respect to the x-axis, the left/right-handed CLC superstructure will endow a geometric phase of $+2\alpha/-2\alpha$ into the reflected light, respectively,[26−28] whereas the light with the opposite handedness of the CLC will directly transmit without such geometric phase modulation.[46]

Based on this principle, a distorted grating is delicately designed and imprinted in both left- and right-handed superstructures. The director orientation α at surfaces is depicted in Figure 1c, which guides the standing CLC helixes to rotate continuously and periodically. The geometry of such a distorted grating can be analogized by bending the straight grating lines of a traditional gradient-phase grating to concentric arcs, and the director orientation is as follows

$$\alpha = \frac{\pi}{\Lambda}\sqrt{x^2 + (y - y_0)^2} \tag{1}$$

where Λ is the grating period and y_0 is the displacement of the curvature center. Here, we pick the values of $\Lambda = 100$ μm and $y_0 = -1.6$ mm. To clarify the principle of OAM detection, the transmission function of the left-handed CLC superstructure is

https://doi.org/10.1021/acsphotonics.1c02017
ACS Photonics 2022, 9, 1050−1057

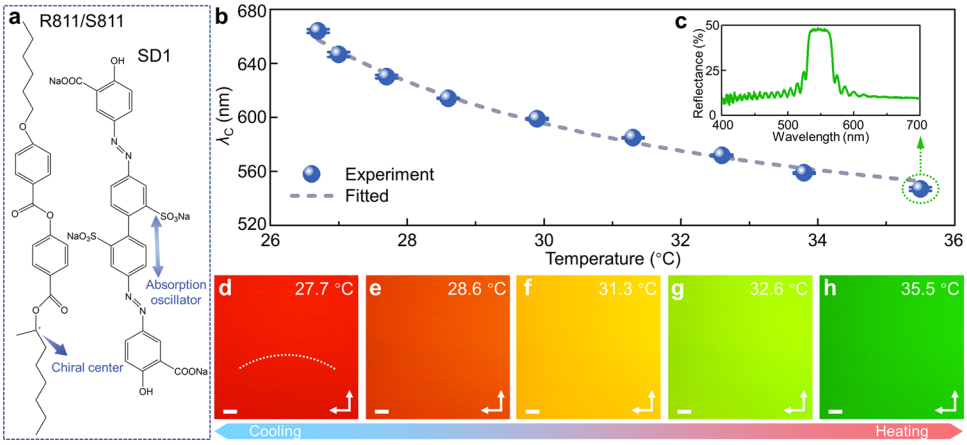

Figure 2. Thermal-controlled chiral superstructures. (a) Molecular structures of the thermoresponsive right/left-handed chiral dopant R811/S811 and the photoalignment agent SD1. (b) Dependency of the central wavelength of the photonic band on the temperature of the left-handed CLC detector. The blue dots with error bars are experimental results, while the gray dashed line is the fitted curve based on Keating theory. (c) Reflectance spectrum at 35.5 °C. (d–h) Reflective polarized optical micrographs of the left-handed CLC detector at (d) 27.7 °C, (e) 28.6 °C, (f) 31.3 °C, (g) 32.6 °C, and (h) 35.5 °C, respectively. The white dashed line indicates arcuate patterns corresponding to the designed distorted grating. The white arrows indicate the polarization direction of the polarizer and the analyzer. All scale bars are 100 μm.

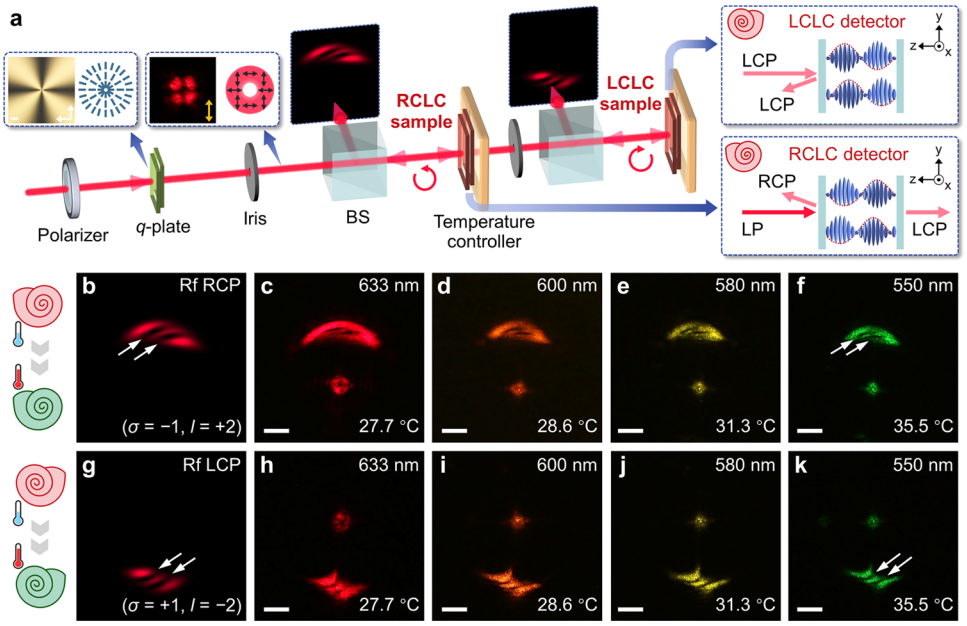

Figure 3. Joint detection of SAMs and OAMs at various wavelengths. (a) Schematic illustration of the optical setup. BS, nonpolarizing beam splitter; RCLC/LCLC, right/left-handed CLC; and LP, linearly polarized light. Inset: the polarized optical micrograph (scale bar: 100 μm) and theoretical director distribution of a nematic LC q-plate with $q = +1$; the transformed patterns after a polarizer (yellow arrow) and the polarization distribution (black arrows) of the incident vector beam from the q-plate; the anticlockwise/clockwise red arrow indicating RCP/LCP light, respectively; the side-view of right/left-handed CLC samples with polarization states of the incident, reflected, and transmitted light labeled, respectively. (b, g) Simulated and experimental reflected diffraction patterns from the right- and left-handed CLC detector at (c, h) 27.7 °C, 633 nm, (d, i) 28.6 °C, 600 nm, (e, j) 31.3 °C, 580 nm, and (f, k) 35.5 °C, 550 nm. The scale bars are 5 mm. The illustration on the left side denotes the blue shift of the operating wavelength along with the temperature increasing. The number of dark fringes is marked by white arrows.

deduced, for instance, under a loose approximation ($|y_0| \gg |x|, |y|$)

$$t(x, y) = \exp\ (+i2\alpha) \approx \exp\left[+i\frac{2\pi|y_0|}{\Lambda}\left(1 + \frac{x^2}{2y_0^2} + \frac{y}{|y_0|}\right)\right]$$

$$= \exp\left[+i\frac{2\pi}{\Lambda}(y + |y_0|)\right] \times \exp\left(+i\frac{\pi x^2}{\Lambda|y_0|}\right) \equiv t_1 \times t_2 \quad (2)$$

where t_1 represents a typical linear phase gradience, contributing to the steering of the diffracted light to the negative direction of the y-axis, t_2 is the quadratic phase term and introduces astigmatism in the incident optical vortex.[47,48] Accordingly, the helical wave front with the topological charge l is transformed to an optical field with $|l|$ intensity nulls on the tilted profile, whose direction is associated with the sign of l. Thus, the number and tilt direction of these dark fringes in the converted pattern can serve as the criteria for OAM detection. For the right-handed CLC, the directions of beam steering and

https://doi.org/10.1021/acsphotonics.1c02017
ACS Photonics 2022, 9, 1050−1057

tilted dark fringes are basically reversed. Therefore, simultaneous detection of SAMs and OAMs can be realized by imprinting this distorted grating into cascaded CLC superstructures with opposite chirality.

To endow these detectors with tunability and controllability, thermoresponsive CLC materials are further introduced as a convenient, practical, reliable, and generally available tool by mixing nematic LC E7 with a chiral dopant R811/S811 (Figure 2a).[49] Based on the photosensitive azo-dye SD1 (Figure 2a) featuring the dichroic absorption and the photoisomerization, the dynamic photopatterning technology[41] (Supporting Information Text 2) is utilized to encode the designed distorted grating (Figure 1c). After the CLC material was capillary-filled into the patterned cell, the initial and terminal orientations of chiral helixes are directed by the adjacent photoalignment layer on substrates. Meanwhile, LC molecules self-assemble into the helixes induced by the interaction of the chiral dopant, thus forming the pre-designed chiral superstructures in a short time. Then, it is mounted on a hot stage to measure the temperature dependency of the Bragg reflection band. Take the left-handed CLC as an example, whose results are plotted in Figure 2b. With the temperature increasing from 26.7 to 35.5 °C, the central wavelength (λ_C) blue shifts from 664 to 547 nm continuously, which agrees well with the theoretically fitted curve based on Keating theory[50] (Supporting Information, Text 3 and Figure S1). Thermal stimulation causes a stronger twist and shorter helical pitch of self-assembled chiral superstructures, thus contributing to the blue shift of the photonic band. The reflectance spectrum at 35.5 °C is shown in detail (Figure 2c), exhibiting a circular photonic band between 529 and 565 nm. It is worth mentioning that the number of helix turns within the cell (N) should be an integer or a half integer owing to parallel orientations at both boundaries, and hence, the pitch (p) is restricted to discrete values by the relation $p = d/N$ (d is the cell gap).[51] As a result, the photonic band does not shift very smoothly but appears discrete, which exactly provides a tolerance to the thermal fluctuation. Figure 2d–h presents the reflective micrographs of the left-handed CLC detector at different temperatures. Typical Grandjean textures with some regular arcuate patterns are exhibited, consistent with the predesigned orientation (Figure 1c). During the thermal stimulation, uniform brilliant color, which sequentially becomes red, orange, yellow, light-green, and green, matches well with the variant photonic band in Figure 2b. The other right-handed CLC sample behaves similarly (Figures S2 and S3). These indicate that *via* regulating the temperature, the CLC-mediated detectors can operate at different wavelengths within a broadband.

Figure 3a illustrates the optical setup for the function characterization of our proposed CLC detectors. To verify the controllability of the operating wavelength, a supercontinuum laser is utilized as the light source and filtered at different wavelengths (λ = 633, 600, 580, and 550 nm). As a representative example of VVBs, a cylindrical vector beam composed of ($\sigma = -1$, $l = +2$) and ($\sigma = +1$, $l = -2$), generated by a nematic LC q-plate[52] (Supporting Information Text 4), is incident on the cascaded CLC superstructures. After preserving the right- and left-handed CLCs on independent temperature controllers, their photonic bands are both tuned to overlap the incident wavelength, and thus, joint detection is achieved. Thanks to the spin selectivity of CLC chiral nanostructures, the SAM component is indicated simply by the presence or absence of the reflected diffraction patterns, where the number and tilt direction of dark fringes evidently reveal the carried OAM.[48] Figure 3c–f shows diffraction patterns from the right-handed CLC detector at different temperatures, indicating the SAM of $\sigma = -1$ and the corresponding OAM component of $l = +2$, while in Figure 3h–k from the left-handed CLC detector, the converted pattern is deflected downward with $\sigma = +1$ and $l = -2$ verified as well. Experimental results match well with numerical calculations of the Fresnel integral (Figure 3b,g). The abovementioned results confirm that the joint detection of SAMs and OAMs has been high-efficiently accomplished, and the dynamic tunability of chiral superstructures makes it accessible in a wide wavelength range.

In addition to the broadband joint detection, controllably selective detection of the SAM and OAM can also be flexibly achieved for single wavelengths (*e.g.*, 633 nm). Various VVBs are further introduced to be the targets, which are generated by the combination of a polarizer, two different q-plates, and two quarter-wave plates (Supporting Information, Text 5 and Figure S4). For the case of cascaded CLC detectors set at 27.7 °C, joint detection is demonstrated (Figure 4a) since the

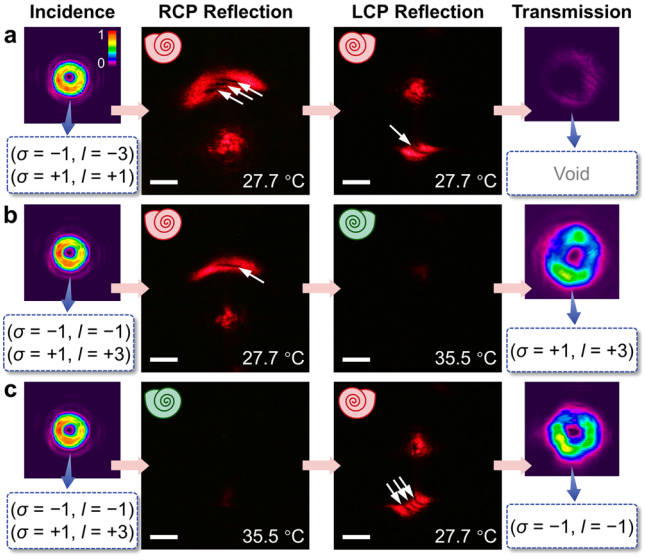

Figure 4. Controllably selective detection of the SAM and OAM at 633 nm. The intensity profiles and SAM/OAM information of the incident/transmitted light and the reflected diffraction patterns from the right/left-handed CLC detectors in (a) joint detection, (b) RCP-selective detection, and (c) LCP-selective detection. The color bar indicates the relative optical intensity. The color of the shell denotes the operating wavelength. The white arrows mark the dark fringes, and the respective temperatures are labeled. All scale bars are 5 mm.

incident light falls within both photonic bands. The reflected diffraction patterns simultaneously show the SAMs of $\sigma = -1$ and $\sigma = +1$ and the OAMs of $l = -3$ and $l = +1$. The captured weak intensity of the finally transmitted light indicates that the incident VVB is almost fully reflected, consistent with the scheme of joint detection. When the temperature of the left-handed CLC superstructure is tuned to 35.5 °C, only the right-handed CLC detector works for another VVB with ($\sigma = -1$, $l = -1$) and ($\sigma = +1$, $l = +3$). As shown in Figure 4b, the RCP component is selectively detected, with one tilted dark fringe indicating the angular momentum information of ($\sigma = -1$, $l = -1$), while the LCP component persists, which is verified by

https://doi.org/10.1021/acsphotonics.1c02017
ACS Photonics 2022, 9, 1050–1057

the absence of the LCP reflection and the donut-shaped intensity profile of the transmitted light. Conversely, when only the left-handed CLC detector operates at 633 nm, (σ = +1, l = +3) data are revealed in Figure 4c, while the orthogonal spin eigenstate passes through the detectors. By independently regulating the temperatures of the cascaded chiral superstructures, the SAM and OAM of light can be selectively identified, and the nondetected component can preserve in the transmitted light for next-step information transferring. In particular, these processes can be dynamically controlled in a reversible way, supplying a promising strategy for *in situ* and nondestructive modulation of angular momenta of light.[46]

To further enhance the thermoresponsivity and extend the tuning wavelength range, a higher concentration of chiral dopant can be rationally adopted since the chirality and responsivity of CLC superstructures are induced by the interaction between the chiral molecules and nematic host.[7] The optimized CLC samples are fabricated and employed for the detection of blue light. Figure 5a displays the reflective

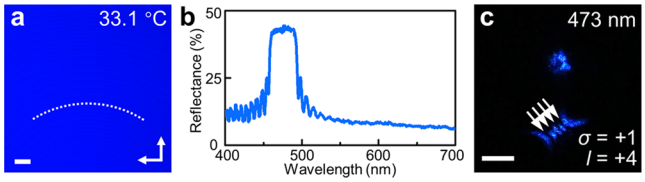

Figure 5. Blue light detection based on CLC superstructures with a higher concentration of chiral dopant. (a) Reflective polarized optical micrograph at 33.1 °C. The white dashed line and arrows indicate regular arcuate patterns and crossed polarizers, respectively. The scale bar is 100 μm. (b) Reflectance spectrum. (c) Reflected diffraction pattern at 473 nm. Dark fringes marked by white arrows indicate l = +4. The scale bar is 5 mm.

micrograph of the left-handed CLC detector at 33.1 °C. Bright and uniform blue color is obviously observed, while periodic arcuate patterns again verify the faithful transformation of the designed pattern (Figure 1c). The corresponding photonic band (457−493 nm) is centered at 475 nm as depicted by its reflectance spectrum (Figure 5b). An optical vortex at 473 nm with a larger topological charge is incident, and the SAM of σ = +1 and the OAM of l = +4 are clearly verified by the reflected diffraction pattern (Figure 5c). This proves a relatively wide spectrum covering nearly the whole visible region for efficient SAM and OAM detection.

CONCLUSIONS

In conclusion, an innovative technique for dynamically selective and simultaneous detection of the SAM and OAM of light is proposed and demonstrated with the collaboration of left- and right-handed thermoresponsive CLC superstructures. Thanks to the spin-determined geometric phase modulation from self-assembled helical nanostructures, the SAM is verified simply by the presence or absence of reflected diffraction patterns, while the OAM is indicated by tilted dark fringes. Based on the thermally tunable photonic band, joint detection of both SAMs and OAMs and selective detection for the intended spin eigenstate are achieved with the merits of controllable wavelength, high efficiency, and good flexibility. Moreover, the preservation of the SAM and OAM information in the transmitted light makes it practical in *in situ* and nondestructive light processing. Actually, dual-band detection of angular momenta of light is also attainable. Such low-cost and easy-fabricated detectors verify the independent and controllable wave front engineering, which can hardly be fulfilled using a conventional single static optical element. In addition to thermoresponsive CLCs demonstrated here, diverse stimuli-responsive chiral nanostructures can also be utilized to implement the proposed scheme. Particularly, light-driven handedness invertible CLCs[53−55] can manipulate orthogonal spin eigenstates, before and after chirality inversion. This work discloses the unprecedented capabilities of self-assembled chiral nanostructures on the stimuli-responsive assembly and interaction with light (especially, the new chiral freedom of light, OAM). The proposed open-ended strategy brings important insights into the architectonics and functionalities of soft chiral nanostructures and might benefit cutting-edge applications in optical manipulation, communications, and diverse intelligent devices beyond optics.

EXPERIMENTAL SECTION

Materials. For the experiment shown in Figures 2−4, the thermoresponsive left-handed CLC was prepared by mixing the nematic LC E7 (HCCH, China) with 25.75 wt % left-handed chiral dopant S811 (HCCH, China), while the right-handed CLC was doped with right-handed chiral dopant R811 (HCCH, China). For the experiment shown in Figure 5, the concentration of the chiral dopant was adjusted to 31.25 wt %. Nematic E7 was also used to fabricate different q-plates.

Sample Fabrication. Indium tin oxide glass substrates were ultrasonically bathed and UV−ozone-cleaned. To form the photoalignment layer, the alignment agent SD1 (Dai-Nippon Ink and Chemicals, Japan) was dissolved in dimethylformamide at a concentration of 0.3 wt %, spin-coated on the substrate, and cured at 100 °C for 10 min. Two pieces of substrates were separated using 7 μm spacers and sealed with epoxy glue to form a cell. The empty cell was placed at the image plane of a digital micromirror device-based dynamic photopatterning system, and a multistep partly overlapping exposure process[41] was performed to accomplish the designed director distributions of the distorted grating or the q-plate (Supporting Information, Text 2). The thermoresponsive CLC material or nematic LC E7 was infiltrated into the corresponding patterned cell at 80 °C and gradually cooled to room temperature, forming a self-assembled CLC distorted grating or an electrically tunable q-plate, respectively.

Characterizations. The CLC samples were mounted on independent temperature controllers (ET-TY115, Etool Technology, China). All micrographs of CLC samples were recorded in the reflective mode of an optical microscope (Nikon 50i POL, Japan) with a crossed polarizer and analyzer. The reflectance spectra were measured with a halogen light source (iDH2000H-HP, ideaoptics, China) and a spectrometer (PG2000-Pro, ideaoptics, China). A supercontinuum fiber laser (SuperK EVO, NKT Photonics, Denmark) filtered at different monochromatic wavelengths using a multichannel acousto-optic tunable filter (SuperK SELECT, NKT Photonics, Denmark) was used for broadband optical characterizations. The reflected diffraction patterns from cascaded CLC detectors illuminated on a screen at a distance of 90 cm and were captured using a digital camera (EOS M, Canon, Japan), while the intensity profiles of the incident/transmitted VVBs were captured using a charge-coupled device (CCD) camera (BGS−SP620, Ophir-Spiricon). A 1 kHz square-wave AC signal output using a function generator (33500B, Keysight

https://doi.org/10.1021/acsphotonics.1c02017
ACS Photonics 2022, 9, 1050−1057

Technologies Inc.) was applied to the nematic LC *q*-plate to maintain the half-wave condition for the incident wavelength, that is, 2.50, 2.83, 3.00, and 3.19 V for 633, 600, 580, and 550 nm, respectively.

■ ASSOCIATED CONTENT

Supporting Information

The Supporting Information is available free of charge at https://pubs.acs.org/doi/10.1021/acsphotonics.1c02017.

Theoretical description of VVBs; description of the azo-dye SD1-based dynamic photopatterning technology; interpretation of Keating theory on thermoresponsivity of chiral superstructures; principles of generating cylindrical vector beams and VVBs *via* *q*-plates; temperature-dependent photonic band and micrographs of the right-handed CLC detector; and optical setup to generate VVBs (PDF)

■ AUTHOR INFORMATION

Corresponding Authors

Peng Chen − *National Laboratory of Solid State Microstructures, Key Laboratory of Intelligent Optical Sensing and Manipulation, College of Engineering and Applied Sciences, and Collaborative Innovation Center of Advanced Microstructures, Nanjing University, Nanjing 210093, China;* orcid.org/0000-0003-3559-8359; Email: chenpeng@nju.edu.cn

Yan-Qing Lu − *National Laboratory of Solid State Microstructures, Key Laboratory of Intelligent Optical Sensing and Manipulation, College of Engineering and Applied Sciences, and Collaborative Innovation Center of Advanced Microstructures, Nanjing University, Nanjing 210093, China;* orcid.org/0000-0001-6151-8557; Email: yqlu@nju.edu.cn

Authors

Yi-Heng Zhang − *National Laboratory of Solid State Microstructures, Key Laboratory of Intelligent Optical Sensing and Manipulation, College of Engineering and Applied Sciences, and Collaborative Innovation Center of Advanced Microstructures, Nanjing University, Nanjing 210093, China*

Chun-Ting Xu − *National Laboratory of Solid State Microstructures, Key Laboratory of Intelligent Optical Sensing and Manipulation, College of Engineering and Applied Sciences, and Collaborative Innovation Center of Advanced Microstructures, Nanjing University, Nanjing 210093, China*

Lin Zhu − *National Laboratory of Solid State Microstructures, Key Laboratory of Intelligent Optical Sensing and Manipulation, College of Engineering and Applied Sciences, and Collaborative Innovation Center of Advanced Microstructures, Nanjing University, Nanjing 210093, China*

Xin-Yue Wang − *National Laboratory of Solid State Microstructures, Key Laboratory of Intelligent Optical Sensing and Manipulation, College of Engineering and Applied Sciences, and Collaborative Innovation Center of Advanced Microstructures, Nanjing University, Nanjing 210093, China*

Shi-Jun Ge − *National Laboratory of Solid State Microstructures, Key Laboratory of Intelligent Optical Sensing and Manipulation, College of Engineering and Applied Sciences, and Collaborative Innovation Center of Advanced Microstructures, Nanjing University, Nanjing 210093, China;* orcid.org/0000-0002-2493-0347

Wei Hu − *National Laboratory of Solid State Microstructures, Key Laboratory of Intelligent Optical Sensing and Manipulation, College of Engineering and Applied Sciences, and Collaborative Innovation Center of Advanced Microstructures, Nanjing University, Nanjing 210093, China;* orcid.org/0000-0003-1255-9453

Complete contact information is available at: https://pubs.acs.org/10.1021/acsphotonics.1c02017

Author Contributions

P.C. and Y.-H.Z. conceived the original idea and designed the experiment. Y.-H.Z. conducted the designs, numerical simulations, and experiments with the assistance of P.C., C.-T.X., L.Z., and X.-Y.W. Y.-H.Z. and P.C. prepared the original article. All authors participated in the discussion and contributed to refining the manuscript. P.C. and Y.-Q.L. cosupervised and directed the research.

Notes

The authors declare no competing financial interest.

■ ACKNOWLEDGMENTS

This work was supported by the National Key Research and Development Program of China (No. 2021YFA1202000), the National Natural Science Foundation of China (NSFC) (Nos. 12004175, 62175101, 62035008, and 62105143), the Natural Science Foundation of Jiangsu Province (Nos. BK20212004, and BK20200311), the Fundamental Research Funds for the Central Universities (No. 021314380185), and the Innovation and Entrepreneurship Program of Jiangsu Province.

■ REFERENCES

(1) Sharma, V.; Crne, M.; Park, J. O.; Srinivasarao, M. Structural Origin of Circularly Polarized Iridescence in Jeweled Beetles. *Science* **2009**, *325*, 449−451.

(2) Scarangella, A.; Soldan, V.; Mitov, M. Biomimetic Design of Iridescent Insect Cuticles with Tailored, Self-Organized Cholesteric Patterns. *Nat. Commun.* **2020**, *11*, No. 4108.

(3) Ren, J.; Wang, Y.; Yao, Y.; Wang, Y.; Fei, X.; Qi, P.; Lin, S. H.; Kaplan, D. L.; Buehler, M. J.; Ling, S. J. Biological Material Interfaces as Inspiration for Mechanical and Optical Material Designs. *Chem. Rev.* **2019**, *119*, 12279−12336.

(4) Wang, L.; Urbas, A. M.; Li, Q. Nature-Inspired Emerging Chiral Liquid Crystal Nanostructures: From Molecular Self-Assembly to DNA Mesophase and Nanocolloids. *Adv. Mater.* **2020**, *32*, No. 1801335.

(5) Kotov, N. A.; Liz-Marzán, L. M.; Weiss, P. S. Chiral Nanostructures: New Twists. *ACS Nano* **2021**, *15*, 12457−12460.

(6) Ryabchun, A.; Bobrovsky, A. Cholesteric Liquid Crystal Materials for Tunable Diffractive Optics. *Adv. Opt. Mater.* **2018**, *6*, No. 1800335.

(7) Zheng, Z. G.; Lu, Y. Q.; Li, Q. Photoprogrammable Mesogenic Soft Helical Architectures: A Promising Avenue toward Future Chiro-Optics. *Adv. Mater.* **2020**, *32*, No. 1905318.

(8) Yeh, P.; Gu, C. *Optics of Liquid Crystal Displays*; Wiley: New York, USA, 1999.

(9) Faryad, M.; Lakhtakia, A. The Circular Bragg Phenomenon. *Adv. Opt. Photonics* **2014**, *6*, 225−292.

(10) Bliokh, K. Y.; Rodríguez-Fortuño, F. J.; Nori, F.; Zayats, A. V. Spin-Orbit Interactions of Light. *Nat. Photonics* **2015**, *9*, 796−808.

(11) Allen, L.; Beijersbergen, M. W.; Spreeuw, R. J.; Woerdman, J. P. Orbital Angular Momentum of Light and the Transformation of Laguerre-Gaussian Laser Modes. *Phys. Rev. A* **1992**, *45*, 8185−8189.

(12) Shen, Y. J.; Wang, X. J.; Xie, Z. W.; Min, C. J.; Fu, X.; Liu, Q.; Gong, M. L.; Yuan, X. C. Optical Vortices 30 years on: OAM Manipulation from Topological Charge to Multiple Singularities. *Light: Sci. Appl.* **2019**, *8*, No. 90.
(13) Forbes, A.; de Oliveira, M.; Dennis, M. R. Structured Light. *Nat. Photonics* **2021**, *15*, 253−262.
(14) Gao, D. L.; Ding, W. Q.; Nieto-Vesperinas, M.; Ding, X. M.; Rahman, M.; Zhang, T. H.; Lim, C. T.; Qiu, C. W. Optical Manipulation from the Microscale to the Nanoscale: Fundamentals, Advances and Prospects. *Light: Sci. Appl.* **2017**, *6*, No. e17039.
(15) Tamura, M.; Omatsu, T.; Tokonami, S.; Iida, T. Interparticle-Interaction-Mediated Anomalous Acceleration of Nanoparticles under Light-Field with Coupled Orbital and Spin Angular Momentum. *Nano Lett.* **2019**, *19*, 4873−4878.
(16) Ni, J. C.; Liu, S. L.; Hu, G. W.; Hu, Y. L.; Lao, Z. X.; Li, J. W.; Zhang, Q.; Wu, D.; Dong, S. H.; Chu, J. R.; Qiu, C. W. Giant Helical Dichroism of Single Chiral Nanostructures with Photonic Orbital Angular Momentum. *ACS Nano* **2021**, *15*, 2893−2900.
(17) Li, Y.; Hong, M. H. Parallel Laser Micro/Nano-Processing for Functional Device Fabrication. *Laser Photonics Rev.* **2020**, *14*, No. 1900062.
(18) Pujals, S.; Albertazzi, L. Super-Resolution Microscopy for Nanomedicine Research. *ACS Nano* **2019**, *13*, 9707−9712.
(19) Wang, J. Advances in Communications Using Optical Vortices. *Photonics Res.* **2016**, *4*, No. B14.
(20) Zhou, H. Q.; Sain, B.; Wang, Y. T.; Schlickriede, C.; Zhao, R. Z.; Zhang, X.; Wei, Q. S.; Li, X. W.; Huang, L. L.; Zentgraf, T. Polarization-Encrypted Orbital Angular Momentum Multiplexed Metasurface Holography. *ACS Nano* **2020**, *14*, 5553−5559.
(21) Erhard, M.; Krenn, M.; Zeilinger, A. Advances in High-Dimensional Quantum Entanglement. *Nat. Rev. Phys.* **2020**, *2*, 365−381.
(22) Zhang, S.; Huo, P. C.; Zhu, W. Q.; Zhang, C.; Chen, P.; Liu, M. Z.; Chen, L.; Lezec, H. J.; Agrawal, A.; Lu, Y. Q.; Xu, T. Broadband Detection of Multiple Spin and Orbital Angular Momenta *via* Dielectric Metasurface. *Laser Photonics Rev.* **2020**, *14*, No. 2000062.
(23) Feng, F.; Si, G. Y.; Min, C. J.; Yuan, X. C.; Somekh, M. On-Chip Plasmonic Spin-Hall Nanograting for Simultaneously Detecting Phase and Polarization Singularities. *Light: Sci. Appl.* **2020**, *9*, No. 95.
(24) Zhao, X. S.; Feng, X.; Liu, F.; Cui, K. Y.; Zhang, W.; Huang, Y. D. A Compound Phase-Modulated Beam Splitter to Distinguish Both Spin and Orbital Angular Momentum. *ACS Photonics* **2020**, *7*, 212−220.
(25) Guo, Y. H.; Zhang, S. C.; Pu, M. B.; He, Q.; Jin, J. J.; Xu, M. F.; Zhang, Y. X.; Gao, P.; Luo, X. G. Spin-Decoupled Metasurface for Simultaneous Detection of Spin and Orbital Angular Momenta *via* Momentum Transformation. *Light: Sci. Appl.* **2021**, *10*, No. 63.
(26) Kobashi, J.; Yoshida, H.; Ozaki, M. Planar Optics with Patterned Chiral Liquid Crystals. *Nat. Photonics* **2016**, *10*, 389−392.
(27) Rafayelyan, M.; Tkachenko, G.; Brasselet, E. Reflective Spin-Orbit Geometric Phase from Chiral Anisotropic Optical Media. *Phys. Rev. Lett.* **2016**, *116*, No. 253902.
(28) Barboza, R.; Bortolozzo, U.; Clerc, M. G.; Residori, S. Berry Phase of Light under Bragg Reflection by Chiral Liquid-Crystal Media. *Phys. Rev. Lett.* **2016**, *117*, No. 053903.
(29) Kobashi, J.; Yoshida, H.; Ozaki, M. Polychromatic Optical Vortex Generation from Patterned Cholesteric Liquid Crystals. *Phys. Rev. Lett.* **2016**, *116*, No. 253903.
(30) Chen, R.; Lee, Y. H.; Zhan, T.; Yin, K.; An, Z. W.; Wu, S. T. Multistimuli-Responsive Self-Organized Liquid Crystal Bragg Gratings. *Adv. Opt. Mater.* **2019**, *7*, No. 1900101.
(31) Chen, P.; Wei, B. Y.; Hu, W.; Lu, Y. Q. Liquid-Crystal-Mediated Geometric Phase: From Transmissive to Broadband Reflective Planar Optics. *Adv. Mater.* **2020**, *32*, No. 1903665.
(32) Xu, C. T.; Chen, P.; Zhang, Y. H.; Fan, X. Y.; Lu, Y. Q.; Hu, W. Tunable Band-Pass Optical Vortex Processor Enabled by Wash-Out-Refill Chiral Superstructures. *Appl. Phys. Lett.* **2021**, *118*, No. 151102.
(33) Tokunaga, S.; Itoh, Y.; Tanaka, H.; Araoka, F.; Aida, T. Redox-Responsive Chiral Dopant for Quick Electrochemical Color Modulation of Cholesteric Liquid Crystal. *J. Am. Chem. Soc.* **2018**, *140*, 10946−10949.
(34) Yuan, C. L.; Huang, W. B.; Zheng, Z. G.; Liu, B. H.; Bisoyi, H. K.; Li, Y. N.; Shen, D.; Lu, Y. Q.; Li, Q. Stimulated Transformation of Soft Helix Among Helicoidal, Heliconical, and Their Inverse Helices. *Sci. Adv.* **2019**, *5*, No. eaax9501.
(35) De Sio, L.; Placido, T.; Serak, S.; Comparelli, R.; Tamborra, M.; Tabiryan, N.; Curri, M. L.; Bartolino, R.; Umeton, C.; Bunning, T. Nano-Localized Heating Source for Photonics and Plasmonics. *Adv. Opt. Mater.* **2013**, *1*, 899−904.
(36) Ranjkesh, A.; Yoon, T. H. Fabrication of a Single-Substrate Flexible Thermoresponsive Cholesteric Liquid-Crystal Film with Wavelength Tunability. *ACS Appl. Mater. Interfaces* **2019**, *11*, 26314−26322.
(37) Zhang, W. X.; Froyen, A. A. F.; Schenning, A. P. H. J.; Zhou, G. F.; Debije, M. G.; de Haan, L. T. Temperature-Responsive Photonic Devices Based on Cholesteric Liquid Crystals. *Adv. Photonics Res.* **2021**, *2*, No. 2100016.
(38) Zheng, Z. G.; Li, Y. N.; Bisoyi, H. K.; Wang, L.; Bunning, T. J.; Li, Q. Three-Dimensional Control of the Helical Axis of a Chiral Nematic Liquid Crystal by Light. *Nature* **2016**, *531*, 352−356.
(39) Qin, L.; Gu, W.; Wei, J.; Yu, Y. L. Piecewise Phototuning of Self-Organized Helical Superstructures. *Adv. Mater.* **2018**, *30*, No. 1704941.
(40) Sleczkowski, P.; Zhou, Y.; Iamsaard, S.; de Pablo, J. J.; Katsonis, N.; Lacaze, E. Light-Activated Helical Inversion in Cholesteric Liquid Crystal Microdroplets. *Proc. Natl. Acad. Sci. U.S.A.* **2018**, *115*, 4334−4339.
(41) Chen, P.; Ma, L. L.; Hu, W.; Shen, Z. X.; Bisoyi, H. K.; Wu, S. B.; Ge, S. J.; Li, Q.; Lu, Y. Q. Chirality Invertible Superstructure Mediated Active Planar Optics. *Nat. Commun.* **2019**, *10*, No. 2518.
(42) Ryabchun, A.; Yakovlev, D.; Bobrovsky, A.; Katsonis, N. Dynamic Diffractive Patterns in Helix-Inverting Cholesteric Liquid Crystals. *ACS Appl. Mater. Interfaces* **2019**, *11*, 10895−10904.
(43) Hou, A. Q.; Chen, H. H.; Zheng, C. W.; Xie, K. L.; Gao, A. Q. Assembly of a Fluorescent Chiral Photonic Crystal Membrane and Its Sensitive Responses to Multiple Signals Induced by Small Molecules. *ACS Nano* **2020**, *14*, 7380−7388.
(44) Zhang, Y. H.; Chen, P.; Ge, S. J.; Wei, T.; Tang, J.; Hu, W.; Lu, Y. Q. Spin-Controlled Massive Channels of Hybrid-Order Poincaré Sphere Beams. *Appl. Phys. Lett.* **2020**, *117*, No. 081101.
(45) Gansel, J. K.; Thiel, M.; Rill, M. S.; Decker, M.; Bade, K.; Saile, V.; Freymann, G. V.; Linden, S.; Wegener, M. Gold Helix Photonic Metamaterial as Broadband Circular Polarizer. *Science* **2009**, *325*, 1513−1515.
(46) Chen, P.; Ma, L. L.; Duan, W.; Chen, J.; Ge, S. J.; Zhu, Z. H.; Tang, M. J.; Xu, R.; Gao, W.; Li, T.; Hu, W.; Lu, Y. Q. Digitalizing Self-Assembled Chiral Superstructures for Optical Vortex Processing. *Adv. Mater.* **2018**, *30*, No. 1705865.
(47) Kotlyar, V. V.; Kovalev, A. A.; Porfirev, A. P. Astigmatic Transforms of an Optical Vortex for Measurement of Its Topological Charge. *Appl. Opt.* **2017**, *56*, 4095−4103.
(48) Zheng, S.; Wang, J. Measuring Orbital Angular Momentum (OAM) States of Vortex Beams with Annular Gratings. *Sci. Rep.* **2017**, *7*, No. 40781.
(49) Tzeng, S. Y. T.; Chen, C. N.; Tzeng, Y. Thermal Tuning Band Gap in Cholesteric Liquid Crystals. *Liq. Cryst.* **2010**, *37*, 1221−1224.
(50) Keating, P. N. A Theory of the Cholesteric Mesophase. *Mol. Cryst.* **1969**, *8*, 315−326.
(51) Kobashi, J.; Yoshida, H.; Ozaki, M. Circularly-Polarized, Semitransparent and Doublesided Holograms Based on Helical Photonic Structures. *Sci. Rep.* **2017**, *7*, No. 16470.
(52) Marrucci, L.; Manzo, C.; Paparo, D. Optical Spin-to-Orbital Angular Momentum Conversion in Inhomogeneous Anisotropic Media. *Phys. Rev. Lett.* **2006**, *96*, No. 163905.
(53) Bisoyi, H. K.; Li, Q. Light-Directed Dynamic Chirality Inversion in Functional Self-Organized Helical Superstructures. *Angew. Chem., Int. Ed.* **2016**, *55*, 2994−3010.

https://doi.org/10.1021/acsphotonics.1c02017
ACS Photonics 2022, 9, 1050−1057

(54) Bisoyi, H. K.; Bunning, T. J.; Li, Q. Stimuli-Driven Control of the Helical Axis of Self-Organized Soft Helical Superstructures. *Adv. Mater.* **2018**, *30*, No. e1706512.
(55) Wang, H.; Bisoyi, H. K.; Urbas, A. M.; Bunning, T. J.; Li, Q. Reversible Circularly Polarized Reflection in a Self-Organized Helical Superstructure Enabled by a Visible-Light-Driven Axially Chiral Molecular Switch. *J. Am. Chem. Soc.* **2019**, *141*, 8078−8082.

https://doi.org/10.1021/acsphotonics.1c02017
ACS Photonics 2022, 9, 1050−1057